

An Efficient Transition Prediction Method Using Neural Network Surrogate Models

Jiahao Wu[1,2], Wenping Song[1,2,*], Han Nie[2,3], Chengpeng Liu[1,2]
[1]Institute of Aerodynamics and Multidisciplinary Design Optimization, School of Aeronautics, Northwestern Polytechnical University, Xi'an, Shaanxi 710072, People's Republic of China
[2]National Key Laboratory of Aircraft Configuration Design, Xi'an, Shaanxi 710072, People's Republic of China
[3]State Key Laboratory of High Temperature Gas Dynamics, Institute of Mechanics ,Chinese Academy of Sciences
* Corresponding author.

Abstract

Natural laminar flow (NLF) technology reduces the skin friction on aircraft surfaces by delaying flow transition and maintaining a large-area laminar flow, which is a highly promising aerodynamic drag reduction technology. An efficient and reliable transition prediction method is a prerequisite for the design of natural laminar flow airfoils. The existing e^N method based on direct linear stability theory (LST) requires artificially specified initial values for solving the stability equations, which heavily relies on expert empirical knowledge, and its robustness and efficiency need to be improved. To overcome the high barrier to entry of the e^N transition prediction method (which demands that users possess specialized theoretical knowledge of stability analysis), as well as its poor robustness and low efficiency when coupled with RANS solvers, this paper develops a neural network surrogate model for the disturbance amplification rate, eliminating the abovementioned difficulties. First, a dataset（166,617samples) is established using the linear stability theory results obtained from the Falkner‑Skan similarity solutions. Second, four key parameters — the boundary layer edge Mach number (M_e), the local Reynolds number (Re_l), the shape factor (H_{12}), and the dimensionless circular frequency of disturbance (ω) — are extracted as inputs, and a multi‑layer perceptron (MLP) neural network surrogate model with disturbance amplification rate as output is built. Furthermore, by integrating the disturbance amplification rate along the flow direction, the *N*-factor curves under different disturbance frequencies are obtained. Combined with the e^N transition criterion, the transition location can be quickly determined. A RANS solver with efficient transition prediction capability is developed by integrating the proposed neural network-based transition prediction method. Taking three typical airfoils under subsonic and transonic conditions as examples, the proposed method is validated. The results are compared with those obtained by the linear stability theory (LST)-based transition prediction method and the radial basic function (RBF)-based transition prediction method. The results show that the error between the transition location predicted by the proposed method and that by the direct linear stability theory method is within 3% of the chord length, indicating good accuracy. Compared with the RBF method, the prediction efficiency is improved by more than 25 times, which verifies the reliability and high efficiency of the proposed method. The neural network-based e^N transition prediction method developed in this paper is suitable for the transition prediction of subsonic and transonic airfoils, and can provide a new efficient and reliable transition prediction method for the design of natural laminar flow airfoils.

Keywords: Efficient transition prediction method, Linear stability theory, e^N-method, Neural network surrogate model, CFD solver

1. Introduction

Energy conservation and emission reduction are central to the development of green aviation [1]. Aerodynamic drag reduction design can significantly lower fuel consumption. According to statistics [2], for every 1% reduction in aerodynamic drag, fuel consumption decreases by approximately 0.75% to 1%, thereby directly reducing greenhouse gas emissions and supporting the aviation industry in achieving its carbon neutrality goals. Natural laminar flow technology, which reduces surface friction drag by delaying flow transition and maintaining extensive laminar flow, represents

a highly promising approach for aerodynamic drag reduction. Owing to its substantial drag reduction potential, laminar flow technology has been recognized by the International Air Transport Association's 2050 Aircraft Technology Roadmap [3] as one of the most promising technologies for next-generation aircraft. Taking a modern wide-body aircraft as an example [4], frictional drag on the wings accounts for approximately 30% of total drag. Traditional low-drag design concepts, such as elliptical wings or supercritical airfoils, primarily focus on reducing induced drag or wave drag and have already been extensively explored. In contrast, natural laminar flow technology, which effectively reduces surface friction drag by delaying flow transition, still holds significant untapped potential for drag reduction.

Although the theory of laminar drag reduction was initially established as early as the 1930s–1940s, it was limited by the aircraft manufacturing technology of that time, which made it difficult to produce laminar airfoils that met the requirements. With improvements in industrial manufacturing capabilities and the growing demand for energy efficiency in civil aviation, the National Aeronautics and Space Administration (NASA) launched the "Aircraft Energy Efficiency" (ACEE) program in the 1970s and conducted flight experiments in the 1980s, successfully demonstrating the existence of extensive laminar flow on wing surfaces under real flight conditions. By the 1990s, breakthroughs in hybrid laminar flow control technology enabled the Boeing 757 to achieve laminar flow coverage of over 50% of the chord length on its wings [5]. Since the 21st century, new engineering breakthroughs have been made in this technology. The engine nacelles of the Boeing 787 airliner, designed with laminar flow control, have achieved extensive laminar flow coverage, marking the first large-scale application of this technology on modern wide-body commercial aircraft [6].

Accurate prediction of the laminar-to-turbulent boundary layer transition is a core challenge in natural laminar flow airfoil design. Turbulent boundary layers increase friction drag, leading to higher energy consumption and emissions. During the design iteration process [7], rapid and reliable transition prediction results are essential for design optimization. Therefore, efficient and robust prediction of the transition location constitutes a key step in the development of new high-efficiency natural laminar flow aircraft. With advances in computational fluid dynamics (CFD), large-eddy simulation (LES) [8] and direct numerical simulation (DNS) [9] have been employed for high-precision studies of flow transition mechanisms. However, these methods demand extremely large computational resources, particularly for complex geometries or high Reynolds number conditions, and their computational efficiency still falls short of meeting the large-scale application requirements in practical engineering scenarios.

In the design optimization of laminar drag reduction for practical engineering problems, two main categories of transition prediction methods [10] have been proposed and validated, including the e^N method based on linear stability theory and the γ-$\widetilde{Re}_\theta$ transition model [11] based on local flow variables. The e^N methods based on stability analysis describe the transition process from the perspective of disturbance evolution, offering strong physical relevance and a solid theoretical foundation. The γ-$\widetilde{Re}_\theta$ transition prediction model couples an intermittency factor (γ) with an empirical correlation based on the momentum thickness Reynolds number (Re_θ) to predict transition phenomena in engineering flows. However, this empirical correlation has certain limitations: the threshold value of Re_θ in the model is calibrated using flat-plate boundary layer experiments, and its empirical correlation is sensitive to parameters such as pressure gradient and freestream turbulence characteristics. Moreover, the model lacks sufficient universality: under non-calibrated conditions such as strong adverse pressure gradients, separated flows, or high freestream turbulence levels, the prediction error increases significantly [12].

Given the advantages of the e^N transition prediction method in reflecting the physical mechanism of transition, it has been widely applied in the inverse design and design optimization of laminar wings/airfoils. This paper investigates a neural network surrogate model based on the e^N method in order to lower its barrier to entry and improve its robustness and efficiency.

For laminar wing/airfoil design, the e^N method based on direct linear stability theory is currently the primary approach for predicting transition location. In 1956, Smith and Van Ingen independently proposed the e^N method based on direct linear stability theory [13] and applied it to transition prediction in two-dimensional incompressible flows. However, this method has certain limitations: First, it requires a very high resolution of the boundary layer. Second, because solving the stability

equations is highly sensitive to input parameters and initial conditions, it demands that researchers possess specialized knowledge on how to converge to the correct eigenvalues. Moreover, linear stability theory requires solving eigenvalue problems, especially when analyzing instability waves with multiple frequencies and wavenumbers, which demands substantial computational resources and high computational time costs. Due to the complexity of LST computations and the high requirements for boundary layer resolution, it is difficult to directly integrate the results into CFD solvers. Furthermore, integrating the LST method with CFD solvers typically requires additional computational steps and post-processing, increasing the complexity and time of the overall computational workflow. Consequently, the existing e^N method based on linear stability theory is inefficient when applied to practical design processes, necessitating a new, efficient, and reliable transition prediction method. Compared to direct linear stability theory, the surrogate model-based e^N method, along with other simplified e^N methods (such as the e^N database method and the e^N envelope method), offers similar advantages. These methods are simple, robust, and fast; they require no prior knowledge or specialized expertise from the user, they directly model the eigenvalue problem rather than using envelope simplifications; and they can be easily extended to account for multiple types of instability waves.

Among them, the surrogate model-based e^N method, which is trained on the dataset consisting of extensive direct stability analysis results, exhibits greater advantages in accuracy and generalization capability compared to the simplified e^N method.

In recent years, artificial neural networks have demonstrated their great potential across various disciplines, naturally attracting the interest of researchers in transition prediction. The ability of neural networks to learn complex nonlinear mappings from data makes them particularly suitable as surrogate models for computationally expensive linear stability theory (LST). Instead of solving the eigenvalue problem of the Orr–Sommerfeld equation repeatedly for each frequency and streamwise station, a properly trained neural network can directly predict the disturbance growth rate from local boundary-layer parameters. This surrogate-based approach preserves the physical foundation of the e^N method while drastically reducing the computational cost and eliminating the need for user-specified initial guesses that often hinder the robustness of direct LST. Consequently, neural networks offer an efficient and robust pathway to integrate stability-based transition prediction into iterative aerodynamic design. Thus, research and application of an efficient transition prediction method employing artificial neural network surrogate models is planned.

Fuller [14] was the first to apply neural network methods to linear stability theory in 1997, using a surrogate model to predict disturbance amplification rates in jet flows. Crouch et al. [15] proposed an artificial neural network method for instability prediction in three-dimensional incompressible boundary layers—using a neural network to model LST—demonstrating that this method is hundreds of times faster than LST in solving disturbance evolution and is more robust. Davin et al. [16] constructed a meta-model using neural network committees to predict laminar-to-turbulent transition. This approach effectively improved prediction speed and reduced computational resource requirements; it is more robust and accurate than single best predictor methods and less dependent on grid refinement. Zafar et al. [17] at Virginia Tech proposed a convolutional neural network (CNN) architecture for modeling second-mode instabilities in high-speed boundary layers. Paredes et al. [18] further extended this method, showing that the neural network not only achieves accuracy comparable to direct linear stability theory but also reduces the sensitivity of stability analysis to the number of grid points within the boundary layer. Zafar et al. [19] used a recurrent neural network (RNN) architecture to directly predict the required N-factor envelope and transition location, achieving a mean transition location error of less than 0.7% of any given wing chord. Chang [20] proposed a multi-layer perceptron (MLP) architecture capable of predicting a complete set of growth rates covering the amplified instability wave spectrum associated with a given base flow profile. Cosin et al. [21] trained a relatively larger, deeper MLP to predict the growth rates and streamwise wavenumbers of TS and CF instabilities, obtaining a Latin hypercube sample dataset for boundary-layer flows over a blended wing-body configuration at high subsonic Mach numbers. In 2024, Hoffman of the German Aerospace Center (DLR) [22] investigated two types of networks—an MLP consisting solely of fully connected layers and a neural network with an additional convolutional part. Evaluations of the models based on FSC test data showed

satisfactory prediction accuracy for both stability types. Moreover, both neural networks were trained only on locally self-similar boundary layer flow data, yet achieved good agreement when applied to real three-dimensional boundary layer flows. The quantification of efficiency gains, however, was not the focus of that study.

Nie Han [23][24] developed a surrogate model based on radial basis function (RBF) interpolation to replace the solution of linear stability equations in the e^N method. While maintaining satisfactory accuracy, this approach significantly reduces the time required for disturbance growth rate prediction compared to direct linear stability theory. Zhang Ershuai et al. [25] proposed a neural network-based linear stability analysis (NN-LSA) method that uses a convolutional neural network (CNN) to predict key parameters (such as frequency, wavenumber, and growth rate) of the most unstable waves in the boundary layer. This provides high-quality initial guesses for the iterative solution of linear stability equations, thereby significantly improving computational efficiency and reducing reliance on empirical judgment. Yu Shenghao et al. [26] developed a neural network model based on radial basis functions and a polynomial response surface model, using boundary layer information from a three-dimensional compressible swept blunt plate as the training dataset. They applied the model to transition prediction for a three-dimensional supersonic swept wing configuration, validating the effectiveness and high efficiency of the established e^N neural network model. Fan Jiakun et al. [27] proposed a CNN-based method for predicting crossflow stationary wave transition on supersonic swept wings. The method automatically extracts spatial features such as boundary layer velocity and temperature profiles using a CNN, maps the disturbance growth rate in conjunction with flow and disturbance parameters, and constructs a transition prediction model suitable for the e^N method, significantly improving prediction efficiency and generalization capability. However, CNN structures are relatively complex and require complete flow profile information, leading to limited efficiency gains during the training and prediction phases, and making integration with CFD solvers in engineering practice more difficult.

This paper develops an efficient and robust transition prediction method for laminar wing design using an artificial neural network as a surrogate model. The remainder of this paper is organized as follows. Section 2 presents the methodology, including the compressible Falkner–Skan equations, linear stability theory, and the multi-layer perceptron architecture. Section 3 demonstrates the application of the proposed method to three typical airfoils under subsonic and transonic conditions, followed by a discussion of the results. Section 4 summarizes the main conclusions.

2. Methodology

2.1 Compressible Falkner-Skan Equations

In this paper, Falkner–Skan equations [28] are solved to provide mean flow for generating stability analysis samples. A compressible form of Falkner–Skan equations is

$$\begin{cases} (Cf'')' + ff'' + \beta_H(S - f'^2) = 0, \\ (CS')' + PrfS' + Pr(\gamma-1)M_e^2 Cf'^2 + \beta_H Pr(\gamma-1)M_e^2 f'(f'^2 - S) = 0, \\ C(S) = \dfrac{\rho\mu}{\rho_e\mu_e} = \sqrt{S}\,\dfrac{T_e + 110.3}{T_e S + 110.3}, \\ C'(S,S') = \dfrac{\partial}{\partial\eta}\left(\dfrac{\rho\mu}{\rho_e\mu_e}\right) = \sqrt{S}\,\dfrac{(-T_e)S'}{(T_e S + 110.3)^2}\dfrac{T_e + 110.3}{T_e S + 110.3} + \dfrac{S'}{2\sqrt{S}}\dfrac{T_e + 110.3}{T_e S + 110.3} \end{cases} \tag{1}$$

whose boundary conditions are

$$\begin{cases} \text{No slip wall}(\eta = 0): f = 0, f' = 0, S' = 0 (\text{or } S = S_w); \\ \text{Farfield}(\eta \to \infty): f' = 1, S = 1 \end{cases} \tag{2}$$

where η is nondimensional normal coordinate and S is total enthalpy. Solution of Falkner–Skan equations can be treated as a boundary value problem and can be performed with a shooting method.

2.2 Linear Stability Theory and eN Method

The theoretical basis of the e^N-transition criterion lies in linear stability theory (LST): a small disturbance is introduced into a stable laminar flow, and its amplification or attenuation is observed along the streamwise direction. If the disturbance is attenuated, the flow remains stable and laminar; conversely, if the disturbance is sharply amplified, the flow state undergoes a transition, ultimately evolving from laminar to turbulent.

The proposed method in this paper focuses on transition prediction for the unstable mode of streamwise two-dimensional Tollmien–Schlichting (T-S) waves, where both the wave angle and the spanwise wavenumber are zero.

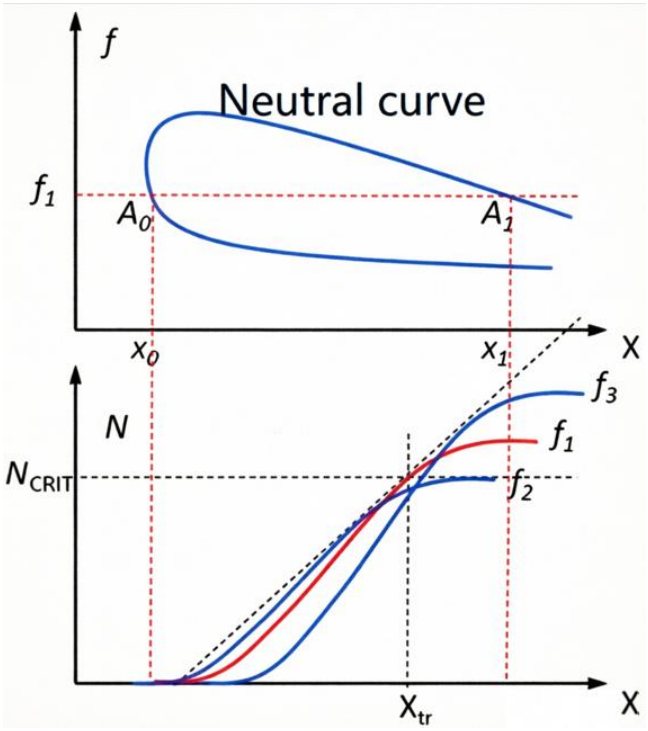


Figure 1 – Schematic of transition prediction using the e^N method

In linear stability theory, transition is considered to occur when the Reynolds number based on boundary layer displacement thickness reaches a critical value and the introduced small disturbance amplifies to e^N times its initial amplitude (typically N is taken as 9, corresponding to an amplification factor of approximately 8000). In this paper, the spatial amplification mode of disturbances is adopted for stability analysis:

For waves of various frequencies, starting from the point where they begin to amplify, their cumulative linear amplification factor is calculated along the downstream direction. Figure 1 illustrates the principle of determining the transition location in a two-dimensional laminar boundary layer using the spatial-mode linear stability theory combined with the e^N method: For a series of dimensional disturbance angular frequencies, the variation of the disturbance growth rate with x is predicted. After non-dimensionalization, starting from the lower branch of the neutral curve (as shown in Figure 1, where the disturbance growth rate at points on the curve is zero; to the left of the curve, the growth rate is negative, meaning disturbances decay; to the right of the curve, the growth rate is positive, meaning disturbances amplify until instability occurs), the following integration is performed:

$$N(x;\Psi=0^\circ,\omega)=\int_{x_0}^{x}\sigma(x,\Psi=0^\circ,\omega)dx=\int_{x_0}^{x}\sigma(x,\beta_s=0,\omega)dx \tag{3}$$

Where ψ is the disturbance wave angle (a value of zero is equivalent to a spanwise wavenumber β_s =0), and ω is the angular frequency. Thus, the corresponding N value at each streamwise position is obtained. The above integration is performed for the disturbance growth rate at each frequency, and then the maximum N-factor at each position is obtained as follows:

$$N(x) = \max\left(\int_{x_0}^{x} \left(-\alpha_i^*\right)_{f=f_n} dx\right) \tag{4}$$

After obtaining the *N*-factor curve, the intersection point with $N=N_{tr}$ is found, and the corresponding *x/c* is the transition location.

2.3 Transition Prediction Method Using Surrogate-Based Stability Analysis

The surrogate-based stability analysis and transition prediction method is implemented in three steps. The first step is to train surrogate models with precalculated samples, that is, eigenvalues of perturbations computed by linear stability analysis. The second step is to use the surrogate model to predict the growth rates of disturbances at different frequencies under a certain flow condition. The third step is similar to a standard e^N method, which integrates the growth rates of perturbations into amplification factors *N* and locates the transition position where *N* factor reaches a prescribed threshold N_{tr}. For more details, please see Ref [24].

2.4 Multi-Layer Perceptron

A multi-layer perceptron (MLP) is a classic feedforward artificial neural network that models complex data relationships through multi-layer nonlinear transformations. Characterized by a concise structure, the MLP can be easily integrated with CFD solvers. The neural network proposed in this paper consists of 6 fully connected layers, with the number of neurons in each layer being 4-512-1024-1024-512-1. The Gaussian Error Linear Unit (GELU) is selected as the activation function, and its mathematical expression is given by:

$$GELU(x) = x \cdot \Phi(x) \tag{5}$$

where $\Phi(x)$ denotes the cumulative distribution function of the standard normal distribution.

3. Results and Discussion

3.1 Validation of the Direct LST-Based eN Method

NLF0416 is a typical natural laminar flow airfoil designed for low-speed aircraft, aiming to reduce friction drag by extending the laminar flow region. In this paper, the e^N transition prediction method based on direct linear stability theory (LST) is used to predict transition for the NLF0416 airfoil over an angle of attack range from -6° to 2°, at a freestream Mach number M_∞=0.1 and a unit Reynolds number Re=4×10^6/m. The *N*-factor threshold is taken as 9, following the results of Stock [29]. A comparison with experimental results from NASA under the same conditions [30] is shown in Figure 2:

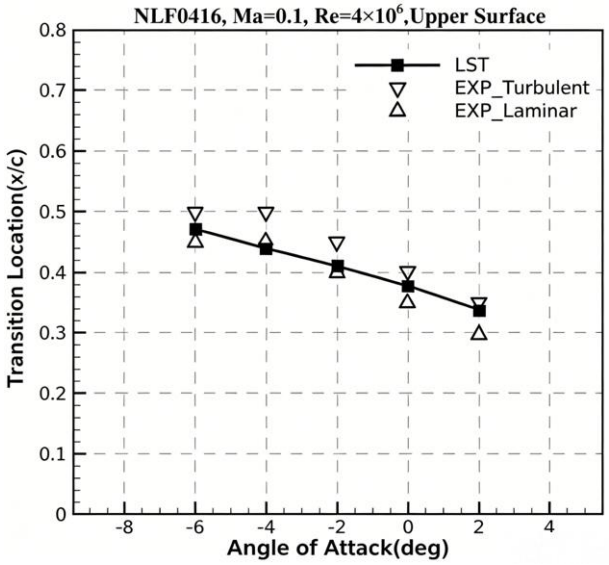


Figure 2 – Comparison of transition locations predicted by direct LST-based e^N method with experimental data

It can be seen that the transition positions calculated by this method are in good agreement with

the experimental results, demonstrating that direct linear stability analysis is feasible for generating training sample sets for surrogate models.

3.2 Data Generation and Preprocessing

Previous research [23] has shown that using only boundary layer edge parameters can achieve modeling performance comparable to using discrete boundary layer profile parameters, while employing edge parameters is more conducive to the subsequent construction of transition models. Therefore, based on the linear stability theory program module of our in-house CFD solver, stability analysis sample points for uniform freestream flow are obtained, which serve as the training set, validation set, and test set for the neural network surrogate model. The input parameters of the artificial neural network surrogate model are the boundary layer edge Mach number Me, shape factor H_{12} , dimensionless angular frequency ω, and local Reynolds number Re_l. The output parameter is the disturbance growth rate α_i. The Falkner-Skan equation is solved as a numerical problem within the boundary layer using the shooting method, followed by direct linear stability analysis. Through uniform sampling, a total of 166,617 sample points are finally obtained for model training. The parameters and their variation ranges are shown in Table 1 below:

Table 1 – Sample parameters and their ranges

Parameter	Varying range	Sampling levels
Me	0.0-1.2	9
H_{12}	2.2-3.5	17
ω	0-0.2	33
Re_l	500-3300	33
α_i	-0.0387389-0.66381	

It is noted that the order of magnitude difference between the upper and lower bounds of ω is significantly larger than that of the other variables (exponential variation), and the distribution of its original values is right-skewed (i.e., many small values, few large values with a wide span). Using the raw values directly would make it difficult for the model to capture the variation pattern, because the influence of small values would be masked by the large values. A logarithmic transformation compresses the exponential variation into a linear one. Therefore, after taking the logarithm separately, a unified Z-score normalization is applied together with the other variables, and the resulting features are then used as input to the neural network for training.

The Multi-Layer Perceptron (MLP) is a classic feedforward artificial neural network that models complex data relationships through multiple layers of nonlinear transformations. The MLP has a simple structure and is easy to integrate with CFD solvers. Therefore, a Multi-Layer Perceptron (MLP) is established, and its structural schematic is shown in Figure 3.

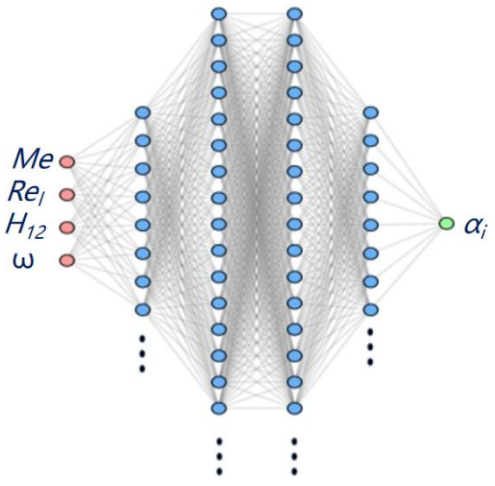


Figure 3 – Architecture of the multi-layer perceptron (MLP) model

The network consists of 6 fully connected layers and adopts a "wide-neck bottle" structure design: the number of neurons in the fully connected layers is 4-512-1024-1024-512-1, enhancing the model's expressive capability through layer-wise compression and expansion. The GELU (Gaussian Error Linear Unit) function is selected as the activation function, which has been explained in detail before.

By combining probabilistic modeling and linear units, the GELU function performs excellently in complex models and large-scale training. Each layer includes batch normalization. The optimizer is AdamW, with a weight decay of 1×10^{-4} serving as L_2 regularization. The initial learning rate is 3×10^{-3}, which decays by a factor of 0.75 every 20 epochs (step decay). The training runs for a maximum of 500 epochs, with an early stopping patience of 50 epochs. The loss function of the model is the Huber loss (with hyperparameter $\delta = 0.05$).

Among the total of 166,617 sample points, 80% are used as the training set, 10% as the validation set, and the remaining 10% as the test set. The model training time is 761.15 seconds. In contrast, the partition strategy for the radial basis function (RBF) surrogate model takes 657.14 seconds. According to reference [23], if a large-scale training set (as used in this paper) is adopted directly, the training time would increase exponentially for RBF surrogate model. The training times for the two methods are shown in Table 2.

Table 2 – Training time comparison of two surrogate models (CPU: Intel i7-14700)

Method	Training Time
MLP	761.15s
RBF	657.14s

The training loss and validation loss descent curves of the model during the training process are shown in Figure 4:

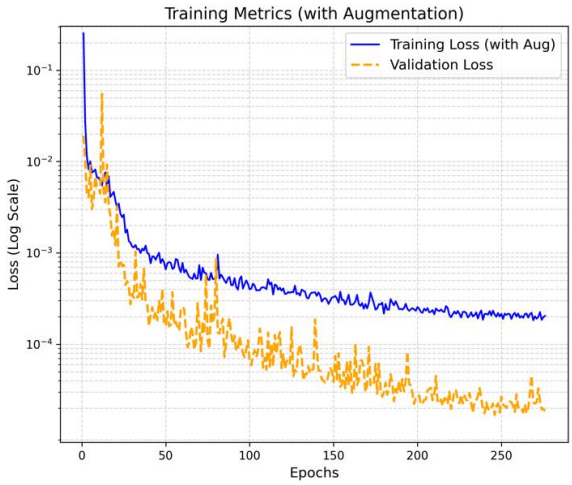


Figure 4 – Training and validation loss curves with data augmentation

During the model training process, data augmentation was used to prevent overfitting—zero-mean Gaussian noise ($\sigma = 0.003$) was added to the inputs of the training set, preventing the model from memorizing specific points and instead forcing it to learn the underlying trend of the data. This implicitly expands the training sample set. The validation set and test set were kept noise-free to ensure that the evaluation metrics reflect the true generalization capability. As a result, the validation loss was lower than the training loss. Therefore, the following comparison shown in Figure 5 is made for the training process:

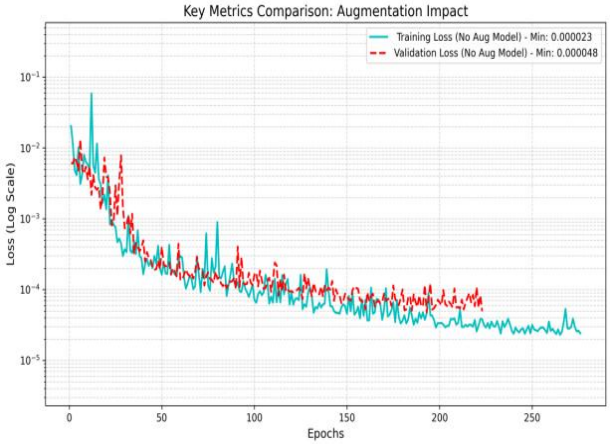


Figure 5 – Training and validation loss curves without data augmentation

As shown in Figure 5, when the model was trained without using data augmentation, the final training loss was lower than the validation loss. The validation loss did not decrease within 50 epochs, triggering the early stopping mechanism, which is consistent with the expected training behavior of a typical neural network. To further demonstrate the advantage of using data augmentation in this paper, a comparison of the validation loss descent curves of the two methods is presented below in Figure 6:

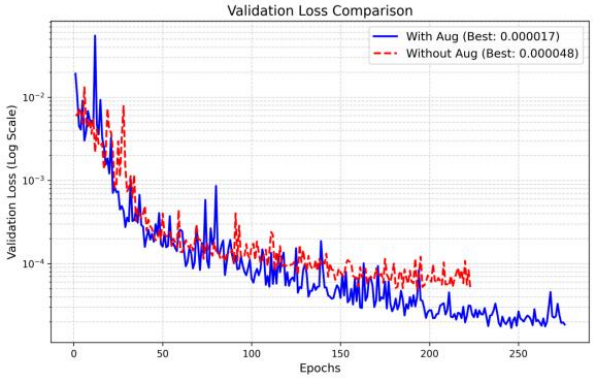


Figure 6 – Comparison of validation loss between two training strategies

It can be seen that, for the same sample set, the validation loss of the model trained with data augmentation is lower than that of the model trained without this technique.

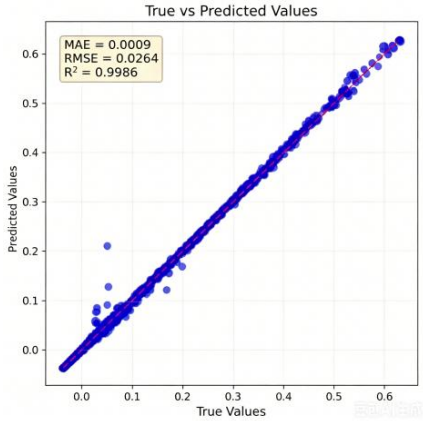


Figure 7 – Comparison of predicted and actual values on test dataset

A comparison between the model-predicted values and the true values on the test set is shown in Figure 7. The coefficient of determination (R^2) of the model is 0.9986, demonstrating that the model

achieves satisfactory predictive performance.

3.3 Coupling the Neural Network Surrogate Model with the RANS Solver

The input parameters of the artificial neural network surrogate model are the shape factor H_{12}, the boundary layer edge Mach number *Me*, the local Reynolds number Re_l, and the dimensionless angular frequency ω These parameters are extracted from the boundary layer solution results and the freestream conditions.

The boundary layer shape factor H_{12} is a dimensionless parameter that describes the shape characteristics of the boundary layer velocity profile, defined as the ratio of the displacement thickness（δ^*）to the momentum thickness (θ):

$$H_{12} = \frac{\delta^*}{\theta} \tag{6}$$

Among them, the displacement thickness and momentum thickness are obtained by integrating the boundary layer velocity profile. For each station on the airfoil, the boundary layer thickness is taken as the distance from the wall to where the dimensionless velocity reaches U_∞. According to the definition, the following integral formulas are applied within this thickness:

$$H_{12} = \frac{\int_0^\delta \left(1 - \frac{u(y)}{U}\right) dy}{\int_0^\delta \frac{u(y)}{U}\left(1 - \frac{u(y)}{U}\right) dy} \tag{7}$$

where y is the distance normal to the upper surface of the airfoil, and $\frac{u(y)}{U}$ is the dimensionless velocity. The boundary layer edge Mach number *Me* can be calculated from the freestream Mach number M_∞:

$$\frac{M_e}{M_\infty} = \frac{U_e}{a_e} \cdot \frac{a_\infty}{U_\infty} \tag{8}$$

From the formula for calculating the speed of sound in air:

$$a = \sqrt{\gamma R T} \tag{9}$$

The formula above is transformed into:

$$\frac{M_e}{M_\infty} = \frac{U_e}{U_\infty} \cdot \sqrt{\frac{T_\infty}{T_e}} \tag{10}$$

Among them, U_e and T_e are obtained from the boundary layer solution, while M_∞ and T_∞ are given by the freestream conditions. The local Reynolds number Rel is then obtained from the following series of formulas:

$$T_{TE} = T_{EFJ} \times T_{INF} \tag{11}$$

For air, using Sutherland's formula:

$$\mu_{INF} = 1.458 \times 10^{-6} \times \frac{T_{INF}^{1.5}}{T_{INF} + 110.4} \tag{12}$$

$$\mu_e = 1.458 \times 10^{-6} \times \frac{T_{TE}^{1.5}}{T_{TE} + 110.4} \tag{13}$$

Among them, T_{TE} is the dimensional boundary layer edge temperature, T_{EFJ} is the dimensionless boundary layer edge temperature, and T_{INF} is the dimensional freestream temperature. Finally, the local Reynolds number is obtained as:

$$\mathrm{Re}_l = \sqrt{\mathrm{Re}_{INF}\, U_e s T_{EFJ}{}^{2.5}\, \frac{\mu_{INF}}{\mu_e}} \tag{14}$$

where Re_{INF} is the freestream unit Reynolds number, U_e is the dimensionless boundary layer edge velocity, and s is the distance from the point along the airfoil surface to the leading edge.

The dimensionless angular frequency is transformed from the dimensional frequency *f* (unit: Hz) through the following series of formulas:

$$\omega^* = 2\pi f \tag{15}$$

According to the definition of local Reynolds number Re_l:

$$\mathrm{Re}\, l = \sqrt{\frac{\rho_e u_e s}{\mu_e}} \tag{16}$$

Then:

$$\rho_e = \frac{R_{el}{}^2 \mu_e}{u_e s} \tag{17}$$

The kinematic viscosity coefficient can be obtained as:

$$\nu_e = \frac{\mu_e}{\rho_e} \tag{18}$$

Then, the local reference length can be obtained as:

$$L = \sqrt{\frac{\nu_e s}{u_e}} \tag{19}$$

Finally, the dimensionless circular frequency is obtained as:

$$\omega = \frac{\omega^* L}{u_e} \tag{20}$$

In the formulas above, u_e is the dimensional boundary layer edge velocity, and *f* is a series of equally spaced frequencies with given upper and lower bounds based on empirical knowledge. Through the above steps, all input parameters required for the neural network have been extracted.

This paper implements the automatic boundary layer transition determination function according to the following steps:

Step 1: Start the RANS calculation with fixed transition. The initial transition location is set as close as possible to the trailing edge of the airfoil to provide a sufficiently large laminar range for the boundary layer transition prediction method. When the flow field solution has essentially converged (based on a pre-specified preliminary convergence criterion for flow field variables or a pre-specified residual convergence criterion), the RANS calculation is temporarily paused, and the computational process enters the airfoil boundary layer transition prediction stage. At this point, the two-dimensional boundary layer edge parameter calculation module is called to analyze the flow field solution, including the pressure distribution on the airfoil surface, flow velocity components, temperature, laminar viscosity coefficient, etc., and to compute the distribution of boundary layer edge parameter values along the streamwise direction required for solving the two-dimensional laminar boundary layer equations.

Step 2: Call the two-dimensional laminar boundary layer equation solution module to compute, at each boundary layer station along the streamwise direction, the velocity profile, temperature profile, and their first and second derivatives normal to the wall surface. At the same time, the laminar separation point is determined from the solution of the laminar boundary layer equations.

Step 3: Call the N_{TS} transition prediction model (neural network surrogate model) based on stability theory to analyze the boundary layer parameters obtained from the boundary layer equations, and compute the streamwise variation curves of the TS wave and the cumulative amplification factor *N*.

Based on the pre-specified transition amplification factor N_{tr}, the boundary layer transition location for the current operating condition is determined.

Step 4: Feed back the latest boundary layer transition information to the RANS solver. Based on the airfoil boundary layer transition information, laminar and turbulent regions can be established in the external flow field around the airfoil. Then, restart the RANS calculation process that was paused in Step 1.

Step 5: Repeat the previous steps (Steps 1 to 4) until the transition location on the airfoil boundary layer no longer changes. At this point, the transition location of the airfoil boundary layer is considered converged, and the flow field calculation process no longer calls the airfoil boundary layer transition prediction module. Continue the iterative solution of the RANS equations based on the converged transition information until the final convergence criterion for the flow field is achieved.

The flow of the RANS solver coupled with the boundary layer transition prediction model is shown in Figure 8.

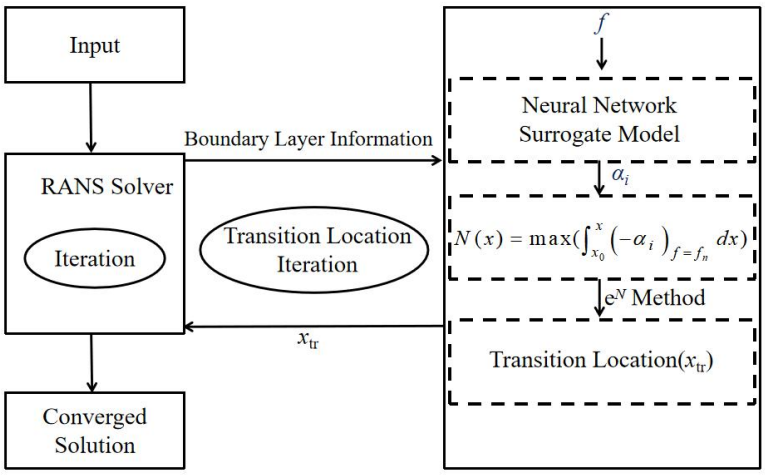


Figure 8 – Flowchart of the RANS solver coupled with the neural network surrogate model

3.4 Efficient Prediction of Airfoil Boundary Layer Transition Based on Neural Networks

3.4.1 Transition Prediction for the Airfoil NLF0416

NLF0416 is a typical natural laminar flow airfoil designed for low-speed aircraft, aiming to reduce friction drag by extending the laminar flow region. In this paper, direct linear stability theory (LST), a radial basis function surrogate model, and an artificial neural network surrogate model (i.e., a multi-layer perceptron, MLP) are used to predict transition for the NLF0416 airfoil over an angle-of-attack range from -6° to 6°, at a freestream Mach number (M_∞ = 0.1) and a unit Reynolds number (Re_∞ = 4×10^6/m). The N-factor threshold follows the results of Stock [28].

To obtain the uniform flow required for stability analysis of the airfoil, the Reynolds-averaged Navier-Stokes (RANS) method is employed, with a prescribed transition location near the trailing edge to ensure a sufficiently large laminar region. A C-type structured grid is used, with 513 grid points circumferentially around the airfoil and 257 points in the wall-normal direction.

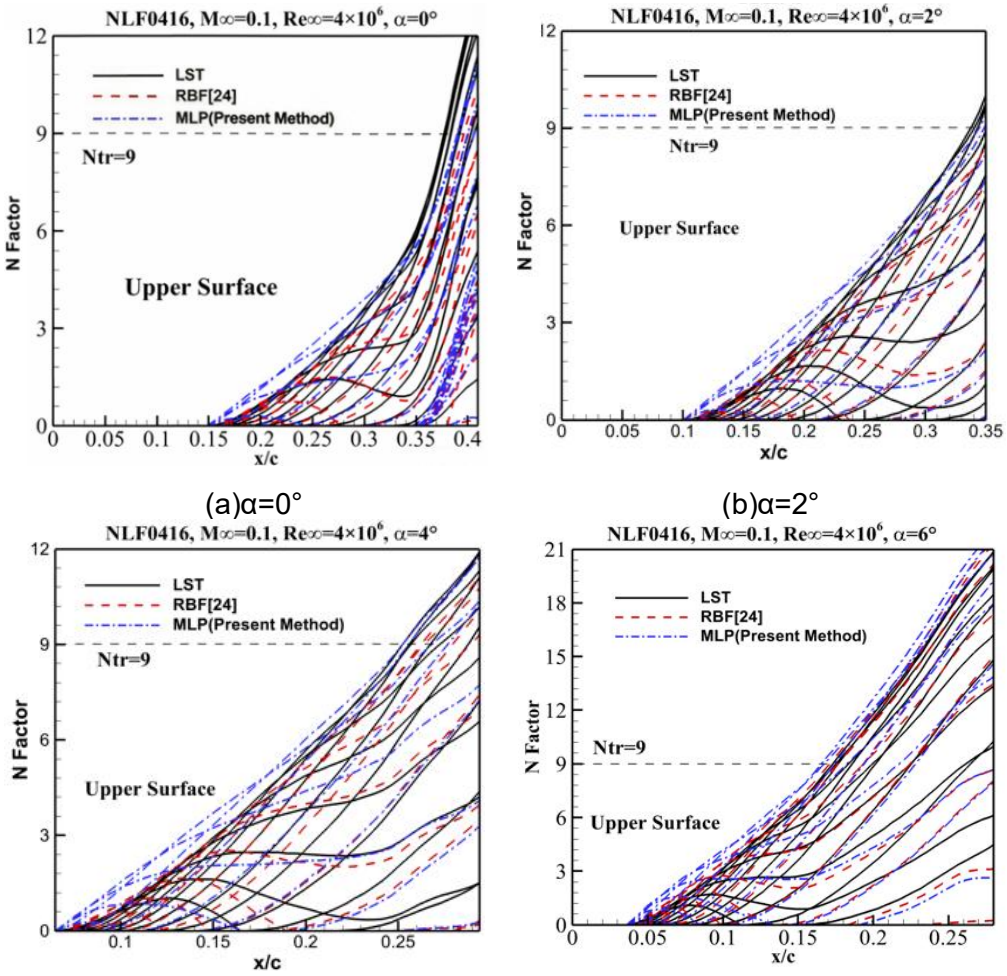
Taking the NLF0416 airfoil at 0° angle of attack as an example, the disturbance growth rate is predicted for 795 input sets on the upper surface. A comparison of the prediction times for the three methods is shown in Table 3.

Table 3 – Transition prediction time comparison of three methods (CPU: Intel i7-14700)

Method	Running time
LST	511.37s
MLP	0.32s
RBF	7.86s

It can be seen that the transition prediction efficiency of the artificial neural network surrogate model is 25 times that of the RBF surrogate model and 1,598 times that of the direct linear stability theory (LST) method, demonstrating the high efficiency of the proposed method.

The predictions of the *N*-factor and transition location on the upper and lower surfaces of the airfoil at different angles of attack using the three transition prediction methods are shown in Table 4 and Table 5, and Figure 9, Figure 10, Figure 11, and Figure 12.



(a)α=0° (b)α=2°

(c)α=4° (d)α=6°

Figure 9 – Comparison of N-factor curves for NLF0416 airfoil (upper surface)

Table 4 – Predicted transition locations at different angles of attack (NLF0416 upper surface)

	-6°	-4°	-2°	0°	2°	4°	6°
Xtr_{LST}/C	0.471325	0.443091	0.416256	0.377392	0.337665	0.252495	0.172948
Xtr_{MLP}/C	0.493402	0.472613	0.438328	0.390159	0.344429	0.252419	0.165525
Xtr_{RBF}/C	0.521097	0.478274	0.456237	0.396468	0.365631	0.262337	0.171050
$\lvert Xtr_{MLP}/C\text{-}Xtr_{LST}/C\rvert$	0.022077	0.029522	0.022072	0.012767	0.006764	0.000076	0.007423
$\lvert Xtr_{RBF}/C\text{-}Xtr_{LST}/C\rvert$	0.049772	0.035183	0.039981	0.019076	0.027966	0.009842	0.001898

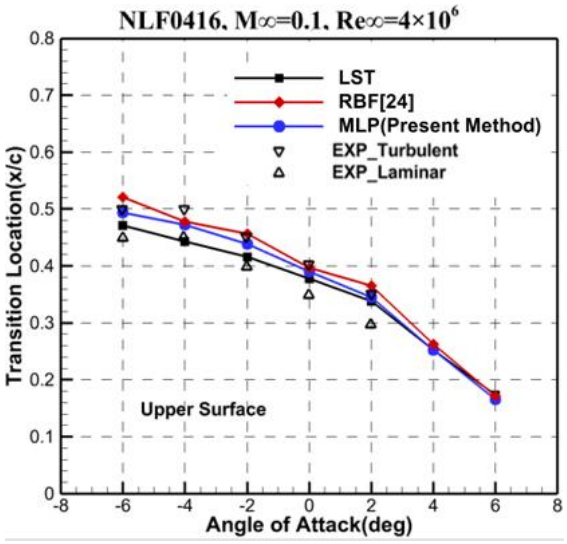
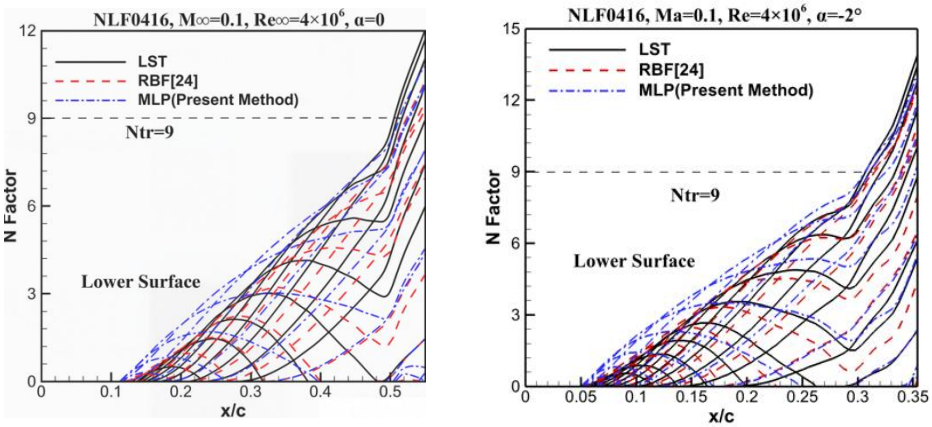


Figure 10 – Predicted transition locations at different angles of attack (upper surface)



a) α =0° b) α =-2°

Figure 11 – Comparison of N-factor curves for NLF0416 airfoil (lower surface)

Table 5 – Predicted transition locations at different angles of attack (NLF0416 Lower Surface)

	-6°	-4°	-2°	0°
Xtr_{LST}/C	0.005519	0.136416	0.307082	0.505185
Xtr_{MLP}/C	0.005519	0.113183	0.306695	0.512684
Xtr_{RBF}/C	0.005519	0.117636	0.313255	0.523126
$\lvert Xtr_{MLP}/C - Xtr_{LST}/C \rvert$	0	0.023233	0.000387	0.007499
$\lvert Xtr_{RBF}/C - Xtr_{LST}/C \rvert$	0	0.018780	0.006173	0.017941

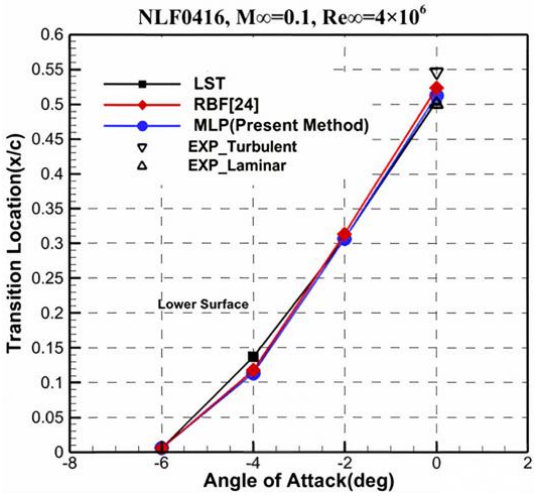


Figure 12 – Predicted transition locations at different angles of attack (lower surface)

The MLP-predicted N-factor curves on both surfaces generally follow the direct LST results, although a slightly larger systematic offset is observed in the N-factor envelopes compared with the RBF surrogate. This difference is likely related to the different approximation characteristics of the two surrogate models: RBF performs local interpolation, whereas MLP provides a globally optimized nonlinear approximation. Small growth-rate differences may accumulate during streamwise integration and become more visible after maximization over disturbance frequencies. Nevertheless, the resulting MLP transition-location differences relative to direct LST remain within 3% of the chord. All three methods also show reasonable agreement with the available experimental transition bounds obtained from the NASA Low-Turbulence Pressure Tunnel [30].

The MLP-predicted transition locations are then passed to the flow solver, with the SA turbulence model applied downstream of transition. Figure 13 shows the resulting skin-friction distributions at the same freestream conditions and an angle of attack of 4°.

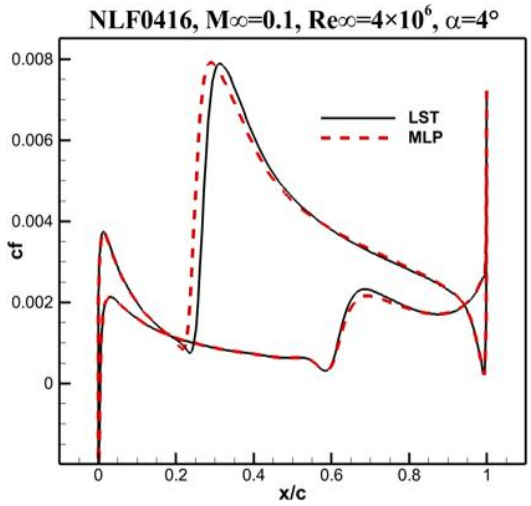


Figure 13 – Comparison of skin friction distributions with predicted transition location

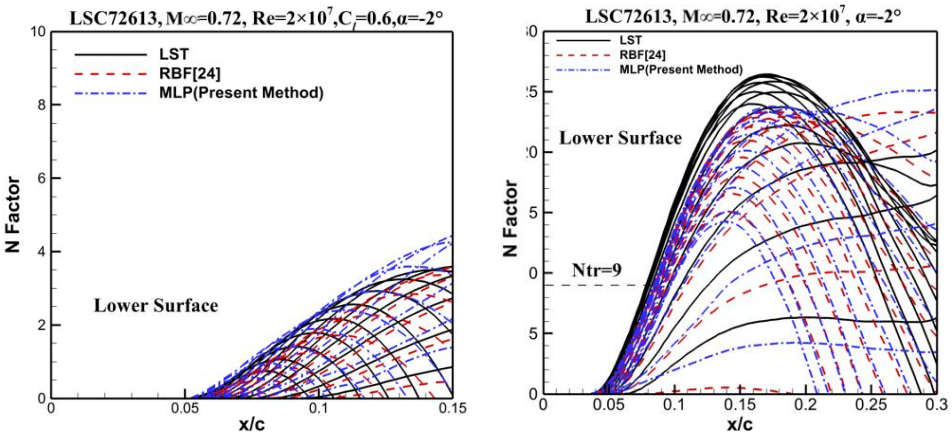
Since turbulence causes a sharp increase in friction drag, by comparing the points where the red and black lines of the friction coefficient begin to rise sharply, it can be seen that the transition points returned by the two transition prediction methods ultimately yield very close flow field calculation results on the upper and lower airfoil surfaces, further demonstrating that the neural network has been integrated with the in-house flow solver PMNS2D.

3.4.2 Transition Prediction for the Airfoil NPU-LSC-72613

The applicability of the proposed method to transonic flows is validated through transition

prediction on the transonic laminar airfoil NPU-LSC-72613. The freestream Mach number M_∞ is 0.72, and the unit Reynolds number is 2×10^7/m. Transition predictions are performed at the design point (C_l=0.6) and several off-design points (angles of attack of -2°, -1.5°, -1°), with the N-factor threshold N_{tr} also taken as 9 [31]. The computational grid has dimensions of 641×257, with 513 grid points distributed circumferentially along the airfoil surface.

Similarly, the N-factor predictions obtained from the neural network (MLP) surrogate model are compared with those from direct linear stability theory (LST) and the radial basis function (RBF) surrogate model. As can be seen from Figure 14 (a), at the design point, due to the strong adverse pressure gradient, the maximum N-factors on both the upper and lower surfaces are lower than the transition threshold. Therefore, the laminar separation point is considered the transition location under this condition. Both MLP and LST return the separation point to the flow field calculation. In this case, the C_f distribution curves obtained by the two methods coincide, and thus are not shown in this paper. Because separation occurs on the upper surface of this airfoil for all operating conditions, LST, RBF, and MLP all return the separation point as the transition location to the flow field calculation; consequently, the predicted transition locations on the upper surface are not presented here. As shown in Table 6 and Figure 15, at the off-design points (angles of attack of -2°, -1.5°, -1° on the lower surface of the airfoil), the transition location predictions from the neural network surrogate model agree well with those from direct linear stability analysis.



(a) C_l=0.6 (b) α=-2°

Figure 14 – Comparison of N-factor curves for LSC-72613 airfoil (lower surface)

Table 6 – Predicted transition locations at different angles of attack (LSC72613 lower surface)

	-2°	-1.5°	-1°
Xtr_{LST}/C	0.078514	0.102321	0.146213
Xtr_{MLP}/C	0.084846	0.106154	0.137132
Xtr_{RBF}/C	0.084928	0.109423	0.152274
$\lvert Xtr_{MLP}/C-Xtr_{LST}/C\rvert$	0.006332	0.003833	0.009098
$\lvert Xtr_{RBF}/C-Xtr_{LST}/C\rvert$	0.006414	0.007102	0.006061

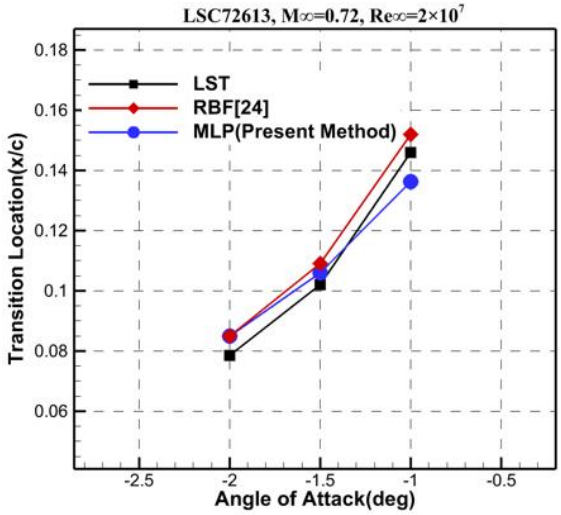


Figure 15 – Predicted transition locations at different angles of attack (LSC72613 lower surface)

Similarly, the transition location returned by the neural network surrogate model is fed into the flow field calculation, and the SA turbulence model is used for the turbulent region downstream of transition. Taking the same freestream conditions and an angle of attack of -2° as an example, it can be observed from Figure 16 that the skin friction coefficient curves on the upper and lower surfaces obtained by the two methods are in good agreement, demonstrating that the transition locations returned by the two transition prediction methods yield very close flow field calculation results on both the upper and lower surfaces.

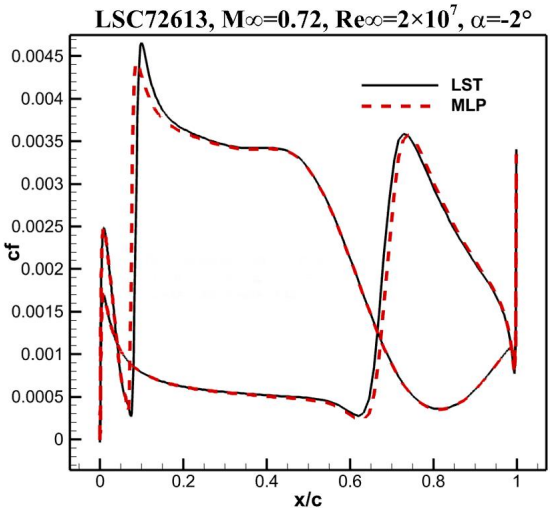
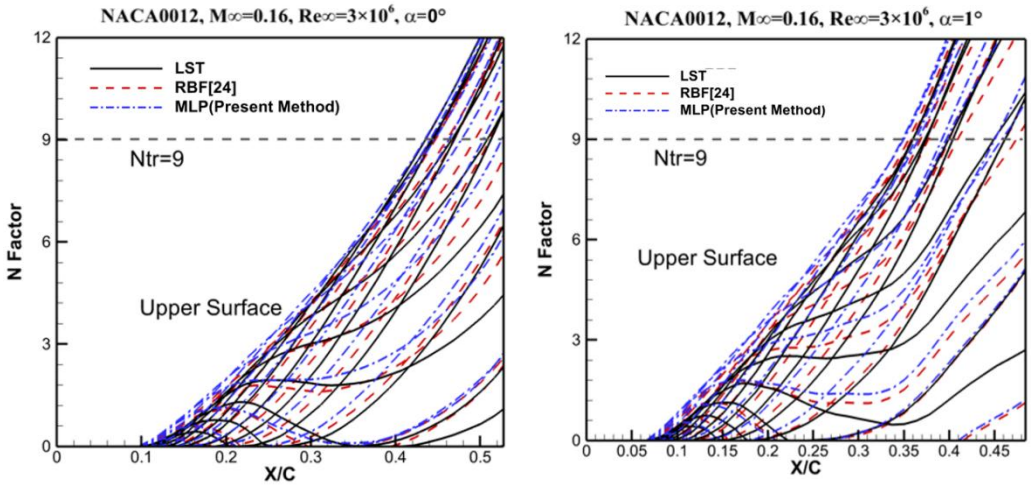


Figure 16 – Comparison of skin friction distributions with predicted transition location

3.4.3 Transition Prediction for the Airfoil NACA0012

To further validate the applicability of the proposed method, transition prediction is performed on the NACA0012 airfoil. The freestream Mach number M_∞ is 0.16, and the unit Reynolds number is 3×10^6/m. Transition predictions are carried out for angles of attack ranging from -3° to 3°. The N-factor threshold N_{tr} is again taken as 9 [32]. The experimental transition location data are taken from Gregory et al. [33]. The computational grid has dimensions of 641×257, with 513 grid points distributed circumferentially along the airfoil surface. The *N*-factor curves obtained by the three methods are shown in Figure 17.



(a) α=0° (b) α=1°

Figure 17 – Comparison of N-factor curves for NACA0012 airfoil

Figure 18 and Table 7 show the transition locations of the NACA0012 airfoil at different angles of attack obtained by the three methods. In this test case, the errors of the transition positions predicted by MLP and RBF compared with those from LST are all within 3% of the chord length.

Table 7 – Predicted transition locations at different angles of attack (NACA0012 upper surface)

	-3°	-2°	-1°	0°	1°	2°	3°
Xtr_{LST}/C	0.672108	0.588013	0.507922	0.435231	0.334035	0.272781	0.196608
Xtr_{MLP}/C	0.688472	0.600102	0.515833	0.434252	0.325249	0.249573	0.170257
Xtr_{RBF}/C	0.676271	0.601242	0.518261	0.440874	0.310986	0.268216	0.210052
$\lvert Xtr_{MLP}/C-Xtr_{LST}/C\rvert$	0.016364	0.012089	0.007911	0.000979	0.023049	0.004565	0.013444
$\lvert Xtr_{RBF}/C-Xtr_{LST}/C\rvert$	0.004163	0.013229	0.010339	0.005643	0.004163	0.013229	0.010339

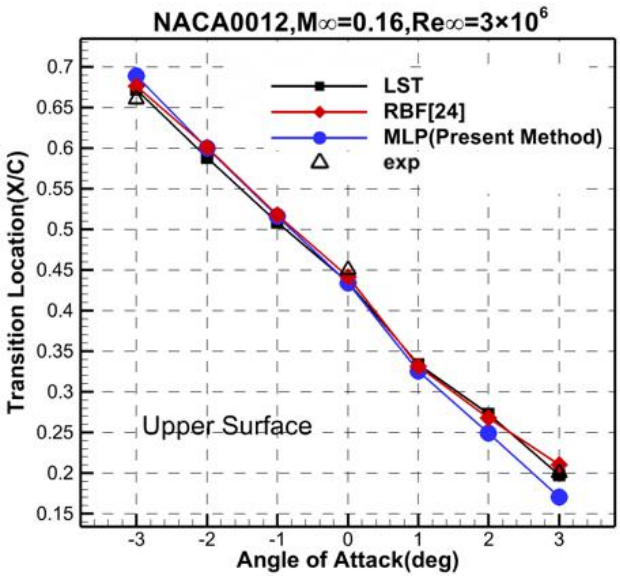


Figure 18 – Predicted transition locations at different angles of attack (NACA0012 upper surface)

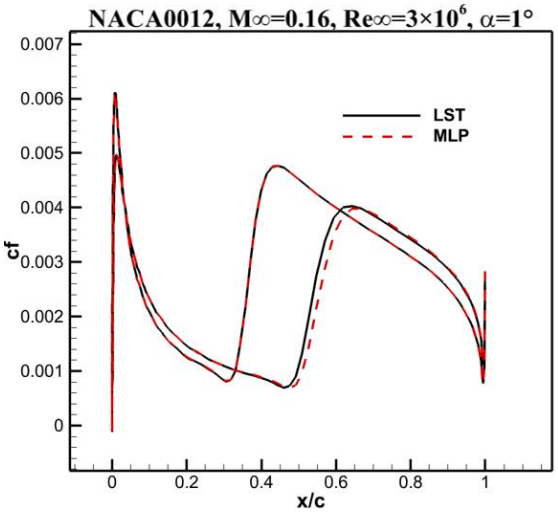


Figure 19 – Comparison of skin friction distributions with predicted transition location

Figure 19 shows the streamwise distribution of the friction coefficient obtained by feeding the transition locations from the two methods back into the flow solver, and the two are in good agreement.

4. Conclusions

This paper focuses on three challenges of the e^N transition prediction method based on direct linear stability theory, namely "lack of robustness, low efficiency, and high requirements for user expertise", and carries out research and application of an efficient transition prediction method using an artificial neural network surrogate model. The main conclusions are as follows:

(1) Stability analysis results based on the similarity solutions of the Falkner-Skan equation are used as training samples. Gaussian noise is artificially introduced for data augmentation, which implicitly expands the sample set, makes more effective use of the existing samples, and performs well on the test set.

(2) The multi-layer perceptron developed in this paper models the solution of the linear stability equations and can be well coupled with the boundary layer base flow calculation method implemented in the fixed-transition RANS approach. The transition locations of three different airfoils are predicted (the difference in transition location compared with the LST method is within 3% chord length in all cases), verifying the reliability and practicality of the proposed method.

(3) This method uses a neural network to model a large amount of data. The training efficiency is comparable to that of the RBF method with partitioned modeling, and the prediction efficiency is significantly improved (25 times that of the RBF surrogate model and 1,598 times that of the direct linear stability analysis method).

Future work will further extend the applicability of the model to three-dimensional complex configurations and high-speed flow conditions, and explore deeper network structures to enhance the model's representational capacity.

5. Contact Author Email Address

wpsong@nwpu.edu.cn

6. Copyright Statement

The authors confirm that they, and/or their company or organization, hold copyright on all of the original material included in this paper. The authors also confirm that they have obtained permission, from the copyright holder of any third party material included in this paper, to publish it as part of their paper. The authors confirm that they give permission, or have obtained permission from the copyright holder of this paper, for the publication and distribution of this paper as part of the ICAS proceedings or as individual off-prints from the proceedings.

References

[1] Ministry of Industry and Information Technology, Ministry of Science and Technology, Ministry of Finance, and Civil Aviation Administration of China. Green aviation manufacturing industry development guidelines (No. [2023]217). 2023.

[2] International Civil Aviation Organization. Carbon offsetting and reduction scheme for international aviation (CORSIA). Montreal: ICAO, 2018.

[3] IATA. Aircraft technology roadmap to 2050[R]. https://www.iata.org/en/publications/technology-roadmap.

[4] Deng Y J, Duan Z Y and Ai M Q. Current status and development of laminar wing design technology. *Acta Aeronautica et Astronautica Sinica*, Vol.43, No.11, pp 526778, 2022.

[5] Collier F S Jr. An overview of recent subsonic laminar flow control flight experiments. AIAA Paper 1993-2987, 1993.

[6] Crouch J D. Modeling transition physics for laminar flow control. AIAA Paper 2008-3832, 2008.

[7] Chen J. Aerodynamic analysis and design of a new transonic natural laminar flow wing. PhD thesis, Northwestern Polytechnical University, 2017.

[8] Urbin G and Knight D. Large-eddy simulation of a supersonic boundary layer using an unstructured grid. *AIAA Journal*, Vol.39, No.7, pp 1288-1295, 2001.

[9] Schlatter S. Assessment of direct numerical simulation data of turbulent boundary layers. *Journal of Fluid Mechanics*, Vol.659, pp 116-126, 2010.

[10] Song W P, Wu M M, Zhu Z, et al. Research on transition prediction method for laminar drag reduction design. *Acta Aerodynamica Sinica*, Vol.36, No.2, pp 213-228, 2018.

[11] Menter F R, Langtry R B, Likki S R, et al. A correlation-based transition model using local variables: part I — model formulation. *Journal of Turbomachinery*, Vol.128, No.3, pp 413-422, 2004.

[12] Langtry R B and Menter F R. Correlation-based transition modeling for unstructured parallelized computational fluid dynamics codes. *AIAA Journal*, 2009.

[13] Smith A M O and Gamberoni N. Transition, pressure gradient and stability theory. Douglas Aircraft Division Rept. ES 26388, Long Beach, CA, 1956.

[14] Fuller R, Saunders W and Vandsburger U. Neural network estimation of disturbance growth using a linear stability numerical model. *Proc. 35th Aerospace Sciences Meeting and Exhibit*, Reno, NV, USA, 1997.

[15] Crouch J D, Crouch I W M and Ng L L. Transition prediction for three-dimensional boundary layers in computational fluid dynamics applications. *AIAA Journal*, Vol.40, No.8, pp 1536-1541, 2002.

[16] Danvin F, Olazabal-Loume M and Pinna F. Laminar to turbulent transition prediction in hypersonic flows with neural networks committee. *Proc. AIAA Aviation 2019 Forum*, Dallas, Texas, 2019.

[17] Zafar M I, Xiao H, Choudhari M M, Li F, Chang C-L, Paredes P, Venkatachari B. Convolutional neural network for transition modeling based on linear stability theory. arXiv preprint arXiv:2005.02599, 2020.

[18] Paredes P, Venkatachari B, Choudhari M M, et al. Toward a practical method for hypersonic transition prediction based on stability correlations. *AIAA Journal*, Vol.58, No.10, pp 4475-4484, 2020.

[19] Zafar M I, Choudhari M M, Paredes P and Xiao H. Recurrent neural network for end-to-end modeling of laminar-turbulent transition. *Data-Centric Engineering*, Vol.2, e17, 2021.

[20] Chang C-L. Development of physics-based transition models for unstructured-mesh CFD codes using deep learning models. *Proc. AIAA AVIATION 2021 FORUM*, 2021.

[21] Cosin R, Mendonca M T, Hanifi A, et al. Deep learning based transition prediction for aeronautical applications. *IUTAM Laminar-Turbulent Transition*, Vol.38, Springer, Cham, pp 725-735, 2022.

[22] Hoffmann J P, Thei A and Hein S. Neural networks as a surrogate model for linear stability analysis of three-dimensional compressible boundary layers. *Proc. AIAA SciTech Forum*, Orlando, FL, 2024.

[23] Nie H. Transition prediction for supersonic boundary layers and natural laminar flow wing design method. PhD thesis, Northwestern Polytechnical University, 2024.

[24] Nie H, Song W P, Han Z H, et al. A surrogate-based e^N method for compressible boundary-layer transition prediction. *Journal of Aircraft*, 2021.

[25] Zhang E S, Liu J X and Huang Z F. Linear stability analysis method based on neural networks. *Acta Aerodynamica Sinica*, Vol.42, No.X, pp 1-15, 2024.

[26] Yu S H, Yuan J S, Gao L J, et al. eN neural network model prediction for three-dimensional supersonic swept-wing transition. *Chinese Journal of Theoretical and Applied Mechanics*, Vol.55, No.6, pp 1236-1246, 2023.

[27] Fan J K, Ai J Q, Xie L, et al. Stationary crossflow induced transition prediction method for supersonic swept-wing based on convolutional neural networks. *Acta Aeronautica et Astronautica Sinica*, Vol.45, No.X, pp XXXXX, 2024.

[28] Schlichting H. *Boundary-layer theory*. McGraw-Hill, New York, pp 344-352, 1979.

[29] Stock H W. Airfoil validation using coupled Navier-Stokes and e^N transition prediction methods. *Journal of Aircraft*, Vol.39, No.1, pp 51-58, 2002.

[30] Somers D M. Design and experimental results for a natural laminar-flow airfoil for general aviation applications. NASA TP-1861, 1981.

[31] Schrauf G. Large-scale laminar flow tests evaluated with linear stability theory. *Journal of Aircraft*, Vol.41, No.2, pp 224-230, 2004.
[32] Johansen J. Prediction of laminar/turbulent transition in airfoil flows. Risø National Laboratory, Roskilde, 1993.
[33] Gregory N and O'Reilly C L. Low-speed aerodynamic characteristics of NACA 0012 aerofoil section, including the effects of upper-surface roughness simulating hoar frost. Reports and Memoranda No. 3726, Aeronautical Research Council, 1970.